Possible Eoarchean records of the geomagnetic field preserved in the Isua Supracrustal Belt, southern west Greenland

Claire I. O. Nichols[a,b,1] (claire.nichols@earth.ox.ac.uk)

Benjamin P. Weiss[a] (bpweiss@mit.edu)

Athena Eyster[c] (ayester@wisc.edu)

Craig R. Martin[a] (crm7@mit.edu)

Adam C. Maloof[d] (maloof@princeton.edu)

Nigel M. Kelly[e] (Nigel.Kelly@bruker.com)

Mike J. Zawaski[f,g] (zawaski@exchange.tamu.edu)

Stephen J. Mojzsis[f,h,i,j] (Stephen.Mojzsis@colorado.edu)

E. Bruce Watson[k] (watsoe@rpi.edu)

Daniele J. Cherniak[l] (dcherniak@albany.edu)

a - Department of Earth, Atmospheric and Planetary Sciences, Massachusetts Institute of Technology, 77 Massachusetts Avenue, Cambridge, MA 02139, USA
b - Department of Earth Sciences, University of Oxford, South Parks Road, Oxford, OX1 3AN, UK;
c - Department of Geoscience, University of Wisconsin-Madison, 1215 West Dayton Street, Madison, WI 53706, USA
d - Department of Geosciences, Princeton University, Guyot Hall, Princeton, NJ 08544, USA
e - Bruker Nano Analytics, 5465 E. Cheryl Parkway, Madison, Wisconsin 53711, USA
f - Department of Geological Sciences, University of Colorado Boulder, UCB 399, Boulder, CO 80309, USA
g - Department of Geology and Geophysics, Texas A&M University, 108 Halbouty Building, 3115 TAMU, College Station, Texas 77843-3115, USA
h - Origins Research Institute, Research Centre for Astronomy and Earth Sciences, MTA Centre of Excellence, 15-17 Konkoly Thege Miklos ut Budapest, 1121 Hungary
i - Department of Lithospheric Research, University of Vienna UZA 2, Josef-Holaubek-Platz 2 A-1090 Vienna, Austria
j - Institute for Earth Sciences, Friedrich-Schiller University Burgweg 11 07749 Jena, Germany
k - Department of Earth and Environmental Sciences, Rensselaer Polytechnic Institute, 110 Eighth Street, Troy, NY 12180, USA
l - Ion Beam Laboratory, State University of New York at Albany, 1400 Washington Avenue Albany, NY 12222, USA

Corresponding author: Claire Nichols

Possible Eoarchean records of the geomagnetic field preserved in the Isua Supracrustal Belt, southern west Greenland

Claire I. O. Nichols[a,b,1], Benjamin P. Weiss[a], Athena Eyster[c], Craig R. Martin[a], Adam C. Maloof[d], Nigel M. Kelly[e], Mike J. Zawaski[f,g], Stephen J. Mojzsis[f,h,i,j], E. Bruce Watson[k], and Daniele J. Cherniak[l]

[a]Department of Earth, Atmospheric and Planetary Sciences, Massachusetts Institute of Technology, 77 Massachusetts Avenue, Cambridge, MA 02139, USA; [b]Department of Earth Sciences, University of Oxford, South Parks Road, Oxford, OX1 3AN, UK; [c]Department of Geoscience, University of Wisconsin-Madison, 1215 West Dayton Street, Madison, WI 53706, USA; [d]Department of Geosciences, Princeton University, Guyot Hall, Princeton, NJ 08544, USA; [e]Bruker Nano Analytics, 5465 E. Cheryl Parkway, Madison, Wisconsin 53711, USA; [f]Department of Geological Sciences, University of Colorado Boulder, UCB 399, Boulder, CO 80309, USA; [g]Department of Geology and Geophysics, Texas A&M University, 108 Halbouty Building, 3115 TAMU, College Station, Texas 77843-3115, USA; [h]Origins Research Institute, Research Centre for Astronomy and Earth Sciences, MTA Centre of Excellence, 15-17 Konkoly Thege Miklos ut Budapest, 1121 Hungary; [i]Department of Lithospheric Research, University of Vienna UZA 2, Josef-Holaubek-Platz 2 A-1090 Vienna, Austria; [j]Institute for Earth Sciences, Friedrich-Schiller University Burgweg 11 07749 Jena, Germany; [k]Department of Earth and Environmental Sciences, Rensselaer Polytechnic Institute, 110 Eighth Street, Troy, NY 12180, USA; [l]Ion Beam Laboratory, State University of New York at Albany, 1400 Washington Avenue Albany, NY 12222, USA

This manuscript was compiled on June 18, 2023

We present paleomagnetic field tests that hint that a record of Earth's 3.7-billion-year (Ga) old magnetic field may be preserved in the banded iron formation from the northeastern Isua Supracrustal belt. Magnetite in the banded iron formation has a Pb-Pb age of 3.7 Ga (1). The U-Pb system has a closure temperature between 150–400°C for the magnetite grain size range observed in the banded iron formation, suggesting the rocks have not been significantly heated since magnetization was acquired. We use a 'pseudo' baked contact test to assess paleodirections in the banded iron formation that have avoided thermal overprints from subsequent igneous intrusions. We demonstrate that specimens that pass this test also go on to pass fold and reversal tests. We argue that the banded iron formation acquired a chemical remanent magnetization via magnetite growth during a multi-phase Eoarchean metamorphic event. We recover what appears to be the oldest known whole rock record of the geomagnetic field, and oldest known records of reversals and secular variation suggesting that Earth's magnetic field behaviour in the Eoarchean may have been similar to that observed today.

Isua | Eoarchean | Geodynamo | Early Earth | Habitability

Recovering a record of the geodynamo throughout Earth history is key to understanding the role of magnetic fields in habitability, the thermal evolution of the early Earth, and the power sources required to sustain planetary dynamos for billions of years. The preservation of a temperate climate and liquid water on Earth's surface has been attributed to the presence of a magnetosphere that shielded the atmosphere from erosion by the solar wind (2). However, recent atmospheric escape models suggest that the presence of a planetary dynamo can enhance escape (3–5). Therefore accurate observations of the intensity of Earth's magnetic field during periods of atmospheric loss will be key for determining the role of a magnetosphere in preserving habitable environments.

The geodynamo currently is driven by compositional convection as the inner core solidifies. However, the age of the inner core remains contentious, with estimates of its initial nucleation ranging from 4.2–0.5 Ga ago (6–11). If the core has a low thermal conductivity (< 100 W m^{-1} K^{-1}), the inner core is predicted to be old (> 1 Ga) and compositional convection could have been sustained throughout much of Earth's history. If the thermal conductivity is high ($100 - 250$ W m^{-1} K^{-1}) and the inner core is young, heat loss would be predominantly via conduction (which would preclude a core dynamo) or else the core underwent compositional convection and sustained a dynamo via precipitation of light elements such as Mg and Si at the core-mantle boundary (12–14). Alternatively, an early core dynamo might have been driven mechanically (e.g., by tides) or else was generated in a basal magma ocean (15, 16). In order to resolve this conundrum, a robust paleomagnetic record that constrains both the strength and stability of the magnetic field before, during and after inner core solidification is required to distinguish between proposed dynamo models.

The aim of this study is to extend the ancient whole-rock paleomagnetic record beyond 3.5 Ga. The previous oldest whole-rock paleomagnetic studies were conducted on rocks from the 3.5 Ga Barberton Greenstone Belt in South Africa and the Duffer Formation, Australia (17–19). A paleointensity of 6.4 μT was recovered from the Duffer Formation (19), although it remains unresolved whether this represents a gen-

Significance Statement

Recovering ancient records of Earth's magnetic field is highly challenging because the magnetization in rocks is often reset by heating during tectonic burial over their long and complex geological histories. We have shown that rocks from the Isua Supracrustal Belt in West Greenland are exceptionally well preserved and have not been substantially heated or deformed since 3.7-billion-years-ago. We have used multiple lines of evidence to demonstrate this, including paleomagnetic field tests which allow magnetic overprints to be identified, the metamorphic mineral assemblages across the area, and the temperatures at which radiometric ages of the observed mineral populations are reset. We show that Earth's magnetic field was broadly similar in strength to today, and discuss the implications of this for habitability and early dynamo generation.

C.I.O.N. and B.P.W. designed research. C.I.O.N., B.P.W., A.E., A.C.M., N.M.K., M.J.Z. and S.J.M. carried out fieldwork. C.I.O.N., and C.R.M. carried out paleomagnetic analyses. C.I.O.N. and B.P.W. interpreted the data. E.B.W. and D.C. carried out diffusion measurements and analysis. C.I.O.N. wrote the paper with feedback from all co-authors.

The authors declare no competing interest.

[1]To whom correspondence should be addressed. E-mail: claire.nicholsearth.ox.ac.uk

uinely weak geomagnetic field record, or inefficient magnetic remanence acquisition. Paleomagnetic studies on single zircon crystals have argued for evidence of an active geodynamo during the Archean and Hadean with a similar field strength to today (20, 21). However, other studies have demonstrated that the magnetic carriers in these zircons are secondary in origin and the magnetization is likely an overprint that post-dates the formation of the zircons by billions of years (22–26). An additional limitation of these single-crystal paleomagnetic studies is that no directional information is preserved (the zircons are detrital). If the mechanism of remanence acquisition can be determined in whole-rock samples, then the age of magnetization could potentially be verified using paleomagnetic field tests, and the stability and intensity of the geomagnetic field can be investigated.

Here, we begin the effort to extend the whole-rock paleomagnetic record to 3.7 Ga ago by recovering natural remanent magnetizations (NRMs) from banded iron formations (BIFs) in the Isua Supracrustal Belt (ISB), southern west Greenland. BIFs have not typically been targeted for paleomagnetic study, and previous results have been hampered by issues with thermal alteration (27, 28). The Isua BIF has an unusually simple mineralogy, comprised of alternating bands of quartz and magnetite with minor amphibole at the boundary between the two phases. The northeast part of the ISB is exceptionally well preserved, with localized regions of low-strain where pillow structures and original sedimentary features are still observable (29). We assessed the potential of the ISB to carry primary Eoarchean paleomagnetic signatures by considering: (i) the thermal history of the area; (ii) the age of magnetization; and (iii) the stability of magnetization.

The paleomagnetic results presented in this study primarily focus on the remanence acquired by magnetite in BIFs. The origin of magnetite in BIFs has been highly debated, although it is now commonly accepted that magnetite is not a primary phase formed directly via precipitation from the water column. The majority of magnetite in BIFs is now considered to be the product of metamorphism and diagenesis of precursor ferro-ferric oxides and hydroxides (30–32). The magnetite in the Isua BIF formed during the 3.69 Ga Eoarchean metamorphic event (1, 33). This age is supported by direct Pb-Pb dating of the magnetite in the Isua BIF, returning an age of ca. 3.69 Ga (1, 34). There is therefore significant uncertainty surrounding the mechanism by which the magnetite in the BIF acquired its paleomagnetic remanence. The magnetite may have grown via direct crystallization, acquiring a grain-growth CRM by growth through a blocking volume (35–37). Alternatively, magnetite may have replaced existing phases in the BIF, acquiring a phase-transformation CRM. The nature of this type of CRM is poorly understood, and in this case is further hampered by the ongoing debate regarding the primary mineralogy in BIFs which could include green rust, ferrihydrite and greenalite (32, 38–40). There is also likely to be a thermal component to the acquired CRM given the high metamorphic and hydrothermal temperatures (450 – 550°C) the magnetite cooled from (1, 33). CRM acquisition over an extended period of time ca. 3.7–3.6 Ga can explain how both normal and reversed directions were captured. However, it is challenging to interpret the paleointensity reported here given the unknown remanence acquisition mechanism and the influence of a potentially reversing field. Nonetheless, it is reasonable to assume that the acquired CRM was less efficient than an equivalent TRM, and averaging over reversals will also act to lower the recovered intensity. Therefore paleointensity estimates recovered from the BIF represent a lower-limit on the true paleointensity at 3.7 Ga.

Three previous studies have investigated the potential of Pb-Pb dating for magnetite (1, 34, 41). These studies were carried out on the Isua BIF, and the Brockman Iron Formation from the Hamersley basin, western Australia. They were motivated by the absence of detrital minerals that are typically used for U-Pb geochronology, such as zircon, apatite and baddeleyite in BIFs (the apatite observed in the Isua BIF is considered to be associated with early hydrothermal events ca. 3.63 Ga (1)). Magnetite contains low but measurable concentrations of U (0.2–0.4 ppm) and Pb (0.2–0.7 ppm) with radiogenic Pb representing $\sim 2\%$ of total Pb (42). The low amount of U and radiogenic Pb makes it challenging to directly recover a U-Pb isochron from magnetite. However, stepwise leaching allowed both uranogenic and thorogenic arrays to be successfully recovered and a Pb-Pb isochron to be calculated.

BIF specimens used to recover the Pb-Pb ages reported in 1 and 34 were collected at 65.20818°N, 49.75855°W, near sites 8A/A, B, C and D in this study. The studies recovered Pb-Pb isochron ages of 3.691 ± 0.049 Ga and 3.691 ± 0.022 Ga and represent the timing of peak temperature metamorphic and metasomatic conditions during the Eoarchean. The Pb-Pb age of the magnetite has not been perturbed or reset since this last metamorphic event. However, previous studies were unable to interpret these ages in terms of the subsequent thermal history of the area, since the Pb diffusion rate in magnetite was unconstrained. Recent Pb diffusion measurements and closure temperature estimates for magnetite (43) allow us to determine that the Pb-Pb age was acquired during a metamorphic event exceeding 120–400°C, consistent with the 450–550°C peak metamorphic temperature of the Eoarchean event recovered from the grunerite-bearing, pyroxene and minnesotaite-absent mineral assemblage in the BIF (33). In addition, our results suggest that the BIF has not been heated to temperatures exceeding 120–400°C in the subsequent Neoarchean and Proterozoic metamorphic events.

The closure temperature of the U-Pb system for magnetite (43) has significant applications for paleomagnetic studies. For thermal remanences, the difference between the closure temperature and the Curie temperature will allow the relationship between the magnetite age and the timing of NRM acquisition to be determined. In addition, for metamorphic rocks where the age of magnetite relative to the age of the bulk rock is often uncertain this technique permits the age of the magnetite, and therefore the oldest possible time of CRM acquisition, to be dated directly.

We conclude that the northernmost region of the northeast ISB has not experienced temperatures above 400°C since 3.69 Ga. We show that the regardless of the mechanism of remanence acquisition, the age of magnetization can be verified by recovering the U-Pb age of magnetite and the timing of any subsequent low-temperature (150–400°C) thermal events will partially or fully reset the U-Pb age. We argue that the magnetite in Isua carries a chemical remanent magnetization (CRM) formed during a complex series of metamorphic and metasomatic events ca. 3.7 Ga (1, 33, 44). For specimens that pass paleomagnetic field tests and exhibit stable demagneti-

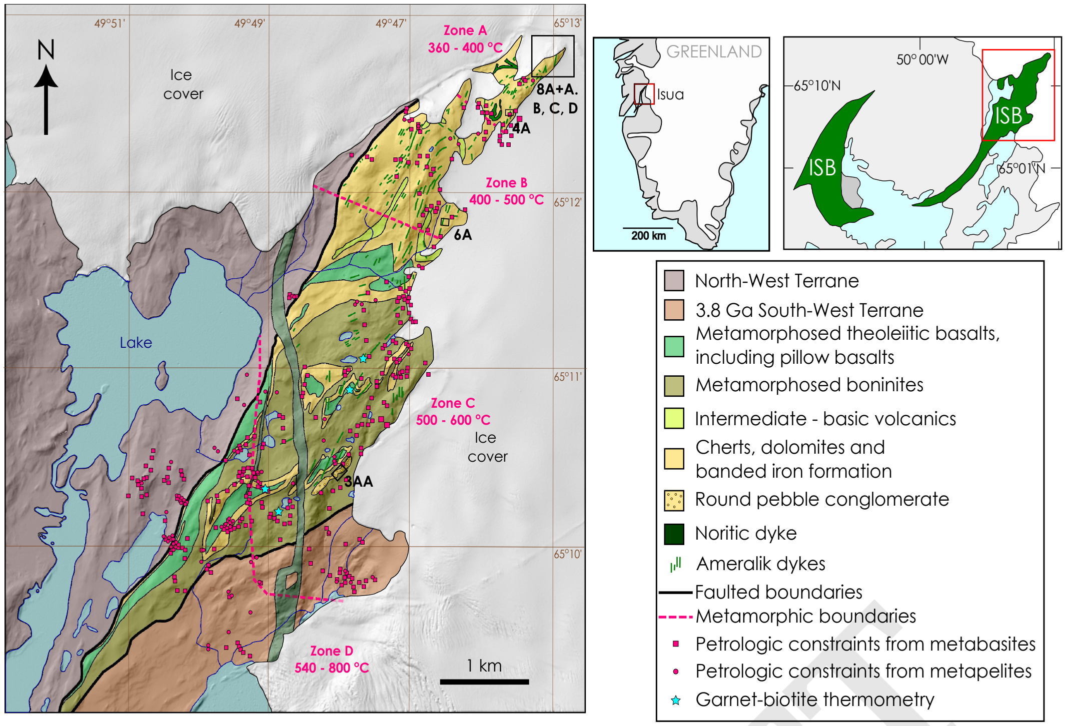

Fig. 1. A simplified geological map (after Nutman et al., 29) depicts the northeastern part of the ISB. The two smaller maps show the entire extent of the ISB and its location in Greenland. The Neoarchean metamorphic event has resulted in a decreasing metamorphic grade across the area constrained by phase equilibrium modelling of metabasites (pink square) and metapelites (pink circles) (45, 46) from south to north. The peak metamorphic temperature has been independently verified using garnet-biotite thermometry at 4 sites shown by the blue stars (47, 48). Isograds between Zones A, B and C which range from lower greenschist in the north to amphibolite grade in the south are shown on the map by the pink dashed lines. The sites where paleomagnetic field tests were conducted are labelled 3AA, 4A, 6A, 8A/A, B, C and D.

zation, pseudo-Thellier experiments yielded a paleointensity estimate of > 15 μT for the Eoarchean geomagnetic field.

Geologic Setting

The northeastern part of the ISB is subdivided into three main terranes separated by faults (Figure 1). The 3.7 Ga northern terrane, the focus of this study, is sandwiched between a northwest terrane to the north and the 3.8 Ga southwest terrane to the south (29). The southern part of the northern terrane is dominated by metamorphosed boninites, interspersed with dolomites, conglomerates, and basalts. Further north in the field area, magnetite-bearing cherts begin to dominate, and the northernmost extent of the area is almost exclusively made up of BIF. Here, we define BIF as the quartz-magnetite formation defined by ref. 33 and the gray-type BIF defined by ref. 49. These 3.7 Ga sediments and volcanics were intruded by dykes that are assumed to be part of the Ameralik dyke swarm, which was emplaced 3.26–3.5 Ga ago across much of the Nuuk district of southwest Greenland(29, 50). The final major intrusive event in the area was the emplacement of a large (> 100 m wide) noritic dyke, which trends north-south across the northeast part of the ISB cross-cutting all the major lithologies (29). Zircons from the dyke have a U-Pb age of 2.214 ± 0.010 Ga (51).

The northern terrane has experienced three significant metamorphic events during the Eoarchean, Neoarchean and Proterozoic. The Eoarchean metamorphic event was followed by an episode of hydrothermal activity 3.63 ± 0.07 Ga ago (52). Two generations of magnetite are observed in the BIF, both of which were formed after primary deposition of Fe-clays such as greenalite (32). The first generation of magnetite that has replaced the primary mineralogy in the original depositional bands yields a Pb-Pb age of 3.69 ± 0.22 Ga (52). A second generation of magnetite is observed as magnetite veins that crosscut the quartz-magnetite banding with a Pb-Pb errorchron of 3.63 ± 0.07 Ga and is attributed to either a contemporaneous or immediately post-metamorphic hydrothermal event (52). Following the Eoarchean metamorphic and metasomatic events, the northern terrane was tilted during juxtaposition against the 3.8 Ga southwest terrane 3.65–3.60 Ga ago (29).

A Neoarchean tectonothermal event impacted Sm-Nd ages in the pillow basalts in the southern part of the region at 2.57 Ga ago (53). The Ameralik dykes were metamorphosed in this event, resulting in the breakdown of olivine, pyroxene and plagioclase to actinolite, chlorite, epidote, albite, serpentine and magnetite (54). These dykes can therefore not be used as part of a traditional baked contact test, since their age of magnetization post-dates the time at which they thermally reset the BIF that they intruded into.

The metamorphic grade during this event decreases from amphibolite facies (< 600°C) in the south closest to the divide between the 3.7 Ga northern and 3.8 Ga southern terranes to greenschist facies (< 380°C) in the most northern part of the 3.7 Ga northern terrane (Figure 1). It has been argued that this is similar to the metamorphic grade progression in a modern-day subduction zone setting (45, 46). We discuss three zones of metamorphism in the field area that relate to the Neoarchean metamorphic event. Zone A experienced peak metamorphic temperatures of 360–400°C and represents the most pristine part of the field area. Zone B experienced peak metamorphic temperatures of 400–500°C. Zone C experienced peak metamorphic temperatures of 500–600°C and is the most metamorphosed part of the area studied. Garnet-biotite thermometry from Zone C independently verifies a peak temperature of 470–550°C during Neoarchean metamorphism (47).

A subsequent thermal perturbation in the Proterozoic (1.5–1.6 Ga ago) is identified by the partial resetting of apatite Pb-Pb ages, and partial homogenization of Rb-Sr in pillow basalts, suggesting peak temperatures < 400°C (53, 55).

Results

We conducted two field campaigns to the ISB between 29th July – 6th August 2018 and 16th July – 27th July 2019. We carried out geological mapping and collected oriented drill core and block samples of a conglomerate and six sites where mafic Ameralik dykes intrude the BIF. A total of three-hundred-and-eight specimens were used for subsequent paleomagnetic analysis.

Paleomagnetic carriers. The NRMs of three lithologies were subjected to thermal demagnetization: conglomeratic clasts (of varying mineralogy, with most being quartz-rich), dolerite dykes (part of the Ameralik dyke swarm) and BIF. Thermal demagnetization shows that for the conglomerate clasts and dolerite, the majority of magnetization is removed between 300–400°C (Figures S16 and S21–28). In the BIF samples, a sharp drop in magnetization close to 580°C suggests the magnetic carrier is magnetite (Figures S21–S28). None of these carriers represent the primary mineralogy and therefore magnetization is interpreted as a TCRM imparted during amphibolite grade metamorphism (450 – 550 °C). Alternating-field (AF) demagnetization removed NRM with an intensity < 0.1 times that for isothermal remanent magnetization (IRM), indicating that specimens have not been lightning remagnetized (Figure S20).

The domain state of magnetite in the BIF was characterized by comparing AF and thermal demagnetization, backfield curves and a Lowrie test (56). Multidomain magnetite was efficiently demagnetized at low field strengths of < 10 mT (57). Both high temperature (HT; > 400°C) and high-coercivity (HC; > 60 mT) directions are similar (Figure S13) although HT directions are slightly influenced by low-coercivity, multidomain overprints which are not effectively removed during thermal demagnetization. Backfield curve acquisition revealed three populations of magnetite grains (Figure S14); the largest population (64–100 % of grains) is dominated by grains with a mean coercivity of $\sim$ 10–20 mT, suggesting they are multidomain. A second population (15–27 % of grains) has a mean coercivity ranging from $\sim$ 60–70 mT and a third population (< 10 % of grains) has a mean coercivity of > 150 mT. These higher coercivity grains are likely stable single domain or single vortex magnetite grains (57). The Lowrie test (Figure S15) showed that AF demagnetization of the NRM was significantly more stable than demagnetization of a 40 mT IRM, indicating that the NRM is primarily carried by stable, single-domain magnetite grains.

Paleomagnetic field tests. In Zone C, a conglomerate test (Site 3AA) was carried out (Figure 1 and S15). Thermal demagnetization of conglomerate clasts revealed stable demagnetization trends at both high (200–300°C) and low (< 200°C) demagnetization temperatures. We define these as components of magnetization for which a paleomagnetic direction can be recovered. Both low and high temperature components (LT and HT) from the conglomerate clasts defined a coherent direction and the hypothesis that they represent a random distribution was rejected with 99% confidence (58). This indicates that the magnetization in the conglomerate post-dates deposition.

Pseudo-baked contact tests (where NRM component directions are compared close to and far from an intrusion, but the intrusion direction itself is not considered) were carried out at two sites in Zone B and four in Zone A. We targeted areas where Ameralik dykes had intruded through the BIF, and therefore represent a distinct, localized thermal perturbation that should only have influenced the BIF immediately adjacent to the dykes. We found that in all cases, the dyke NRM component directions were poorly defined and scattered, with low peak blocking temperatures ($\sim$ 300°C) at each site and between sites suggesting variable CRM acquisition during Neoarchean metamorphism (54) or remanence dominated by multidomain carriers. We therefore focused our attention on identifying systematic changes in the paleomagnetic directions in the BIF with distance from each intrusion.

We infer that the boundary between BIF that was baked and BIF that remained largely unbaked by the dyke intrusion occurs at the distance at which HT components of the NRM begin to converge on a single direction. The width of the baked region was 2.8 dyke radii at site 6A and > 2 dyke radii at Sites 8A, A, B, C and D. The dyke at site 6A is $\sim$ 4 m across, while dykes 8A, A and the dyke which runs through sites B, C and D are $\sim$ 10 m across. The width of the baked region is influenced by a number of factors including the temperature of dyke emplacement, the subsequent cooling-rate of the dyke and the fluid flux into the surrounding BIF. Given that all the dykes are doleritic in composition (29, 54, 59) it is plausible to assume they had similar emplacement temperatures and therefore the width of the contact aureole should increase with dyke width, as we observe.

For each pseudo-baked contact test, Watson's V_W statistic was calculated (60); this statistic determines whether the HT baked and unbaked directions are statistically distinct representing a passed pseudo-baked contact test, or indistinguishable representing a failed test. Three sites (4A, B and D) did not meet our threshold, which we set as recovering baked and unbaked directions that were distinct with 95% confidence (Figure S16). However, at sites 6A, 8A/A and C our pseudo-baked contact tests passed (Figure 2). At Site 6A, the baked region extends out to 5.45 m and HT components (100–375°C) define the direction 249°/56° ($\alpha_{95} = 28°$). In the unbaked region, three specimens with HT components (150–580°C) at distances greater than 5.45 m, and one specimen with a particularly high HT component (475–510°C) that escaped thermal overprinting at a distance of 1.45 m from the intrusion, define the direction 048°/46° ($\alpha_{95} = 25°$). At site 8A/A, BIF specimens taken < 7.3 m from the intrusions exhibit a scattered HT (400–580°C) direction of 187°/-24° ($\alpha_{95} = 59°$). Four BIF specimens taken > 20 m from dyke 8A and > 10 m from dyke A define a HT (400–580°C) direction of 026°/62° ($\alpha_{95} = 47°$). At site C, the baked BIF exhibits a HT (> 500°C) and high coercivity (HC) magnetization direction close to that of the dyke (169°/79°, $\alpha_{95} = 22°$) within 10–20 m of the dyke contact. Further from the intrusion, a distinct HT and HC direction was recovered (294°/25°, $\alpha_{95} = 18°$).

The recovered baked and unbaked BIF directions from the three passed pseudo-baked contact tests were then subjected to a fold test (Figure 3). We gradually un-tilted the recovered geographic directions using the basal bedding measured at each site, and calculated the resulting principal eigenvalue (τ_1) at each step in order to determine the maximum convergence of directions independently of their polarity (61). For the unbaked directions, the maximum value of τ_1 was recovered at $\sim$ 20% untilting, while for the baked directions, the maximum value was recovered for 100% untilting. This suggests that

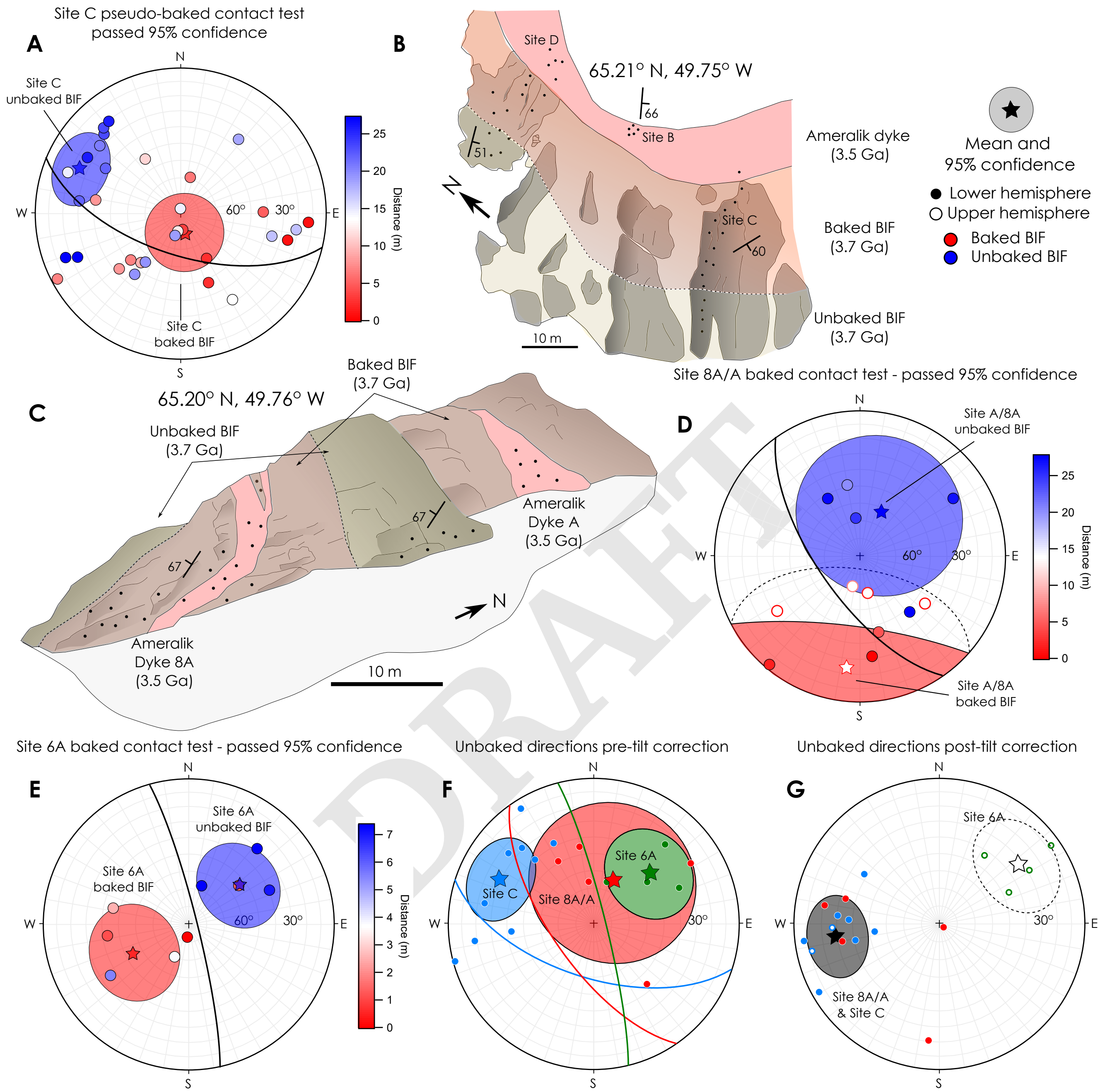

Fig. 2. Passed baked contact tests in geographic coordinates and 3.7 Ga paleodirections in tilt-corrected coordinates. (A) Equal area, lower hemisphere stereoplots showing high temperature (HT) and high coercivity (HC) components recovered for the BIF recovered from Site C. The mean baked BIF direction and unbaked BIF directions are shown by the red and blue stars, respectively. Each recovered paleodirection in the BIF is coloured based on its distance from the dyke contact. (B) An aerial sketch of field sites B, C and D in Zone A. The dyke is shown in red, the baked BIF in orange and unbaked BIF in yellow. (C) An outcrop sketch of site 8A/A. The dykes at site 8A/A are shown in red, the baked BIF is shown in orange and the unbaked BIF in yellow. (D) HT component directions recovered from the baked contact test at sites A and 8A. Each HT direction in the BIF is colour coded with distance from dyke 8A. (E) HT and LT component directions recovered from the baked contact test at site 6A. (F) The HT component directions recovered from the unbaked BIF for each of the passed baked contact tests at site C (blue), site 8A/A (red) and site 6A (green). The directions are shown in geographic coordinates. The basal bedding for each site is shown in the same colour. (G) The HT component directions recovered from the unbaked BIF at each site after tilt correction. The directions from sites C and 8A/A converge (black star) and the direction from site 6A is antipodal (white star). These directions pass a reversal test.

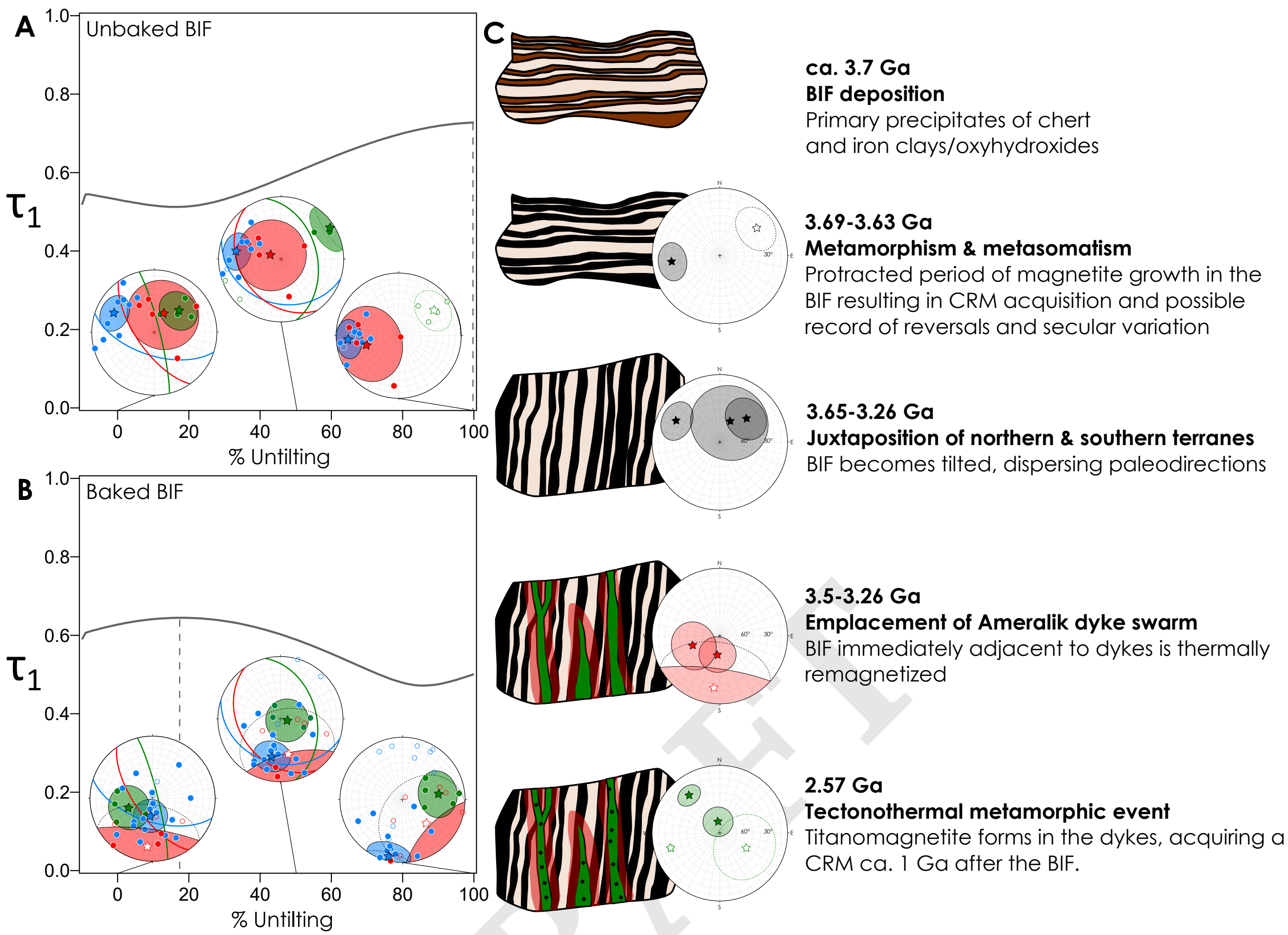

Fig. 3. A fold test and the tilting history of the BIF in the ISB. (A) The principal eigenvalue, τ_1, calculated for all the unbaked BIF directions during various degrees of untilting ranging from -10–100%. The maximum value of τ_1 was recovered for 100% untilting, indicating a passed fold test. The directions for sites 6A, 8A/A and C are shown in green, red and blue, respectively on equal area stereonet projections for 0%, 50% and 100% untilting. (B) As for (A), for baked BIF. The maximum value of τ_1 was recovered at 20% tilting, suggesting Ameralik and thermal remagnetization of the baked BIF was pre- or syn-tilting. (C) A cartoon schematic showing how the the recovered paleomagnetic directions can be interpreted in terms of the geological history of the ISB.

the emplacement of the Ameralik dykes, and the remagnetization of the baked BIF, was pre- or syn-tilting in the region, perhaps during juxtaposition of the northern and southern terranes (29). The tilt-corrected, unbaked BIF directions define two antipodal directions of 263°/29° ($\alpha_{95} = 20°$) and 054°/-31° ($\alpha_{95} = 25°$), respectively (Figure 2g). These antipodal directions pass a reversal test (62; Figure S17).

Pseudo-Thellier paleointensity estimates. We estimated the paleointensity of the Eoarchean geomagnetic field on three specimens of unbaked BIF from sites A and C (Figure S20). Pseudo-Thellier experiments (63) were carried out and AF demagnetization of the NRM revealed a HC component which was origin-trending and stable to > 130 mT. The NRM demagnetization was compared to the AF demagnetization of a 50 μT anhysteretic remanent magnetization (ARM). A preliminary paleointensity estimate of 15.1 $\pm$ 1.2 μT if the NRM represents a TRM (uncertainty is 2 standard deviations) was recovered from all three specimens (Figure 4). One specimen was also corrected for remanence anisotropy (64) which slightly increased the recovered paleointensity to 16.7 $\pm$ 0.7 μT. Since the magnetite in our samples acquired a CRM, these results are taken as evidence for the presence of a field but should not be considered an accurate representation of its strength. CRM acquisition is known to be less efficient than TRM acquisition, but calibrating between the two remains challenging.

The closure temperature of the magnetite U-Pb system. The diffusion rate of Pb was measured in magnetite between 500–700°C and found to have an activation energy, E, of 96.42 kJmol^{-1} and a pre-exponential factor, D_o, of 7.0×10^{-17} m^{2}s^{-1} (43; Figure S1). These values were used to estimate the Dodson closure temperature of the system (i.e., the temperature that the Pb-Pb age of magnetite corresponds to) after cooling from 500°C as a function of grain size and cooling rate, where we allow the cooling rate to vary from 1–100°C Myr^{-1}, covers typical metamorphic cooling rates observed in modern style tectonic settings (75, 76). The average diameter of the magnetite grains in our BIF specimens (1–27 μm) was estimated by comparing the room temperature NRM to the magnetic moment recovered after cooling the specimens to -210°C (77; Supplementary Figure S2) and is supported by the size range observed in scanning electron microscopy (SEM) analysis (Figure S12). For the largest

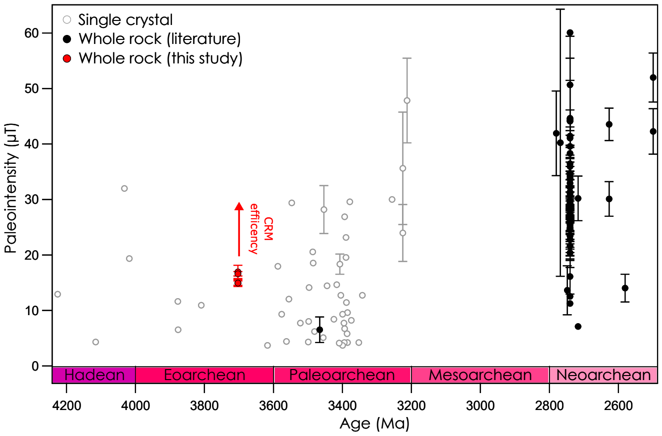

Fig. 4. A summary of previous paleointensity studies throughout the Archean and Hadean compiled by Bono et al., (65). Solid circles represent whole rock studies (19, 66–73) while open circles represent single crystal studies (17, 20, 74). The paleointensities for the three BIF specimens measured here are shown in red. The uncertainty is similar to the size of the circle for the new measurements presented here. The inefficiency of CRM remanence acquisition suggests these intensities likely represent a lower estimate for the Eoarchean geomagnetic field strength (shown by the upward pointing red arrow).

recovered magnetite grains (27 μm), and a cooling rate of 100°C Myr^{-1} the closure temperature is $\sim$ 400°C; this is close to the peak metamorphic temperature in Zone A (Figure S3).

Discussion

Preservation of an ancient magnetic field record in the Isua Supracrustal Belt. We interpret the magnetization in unbaked BIF as a likely record of paleomagnetic remanence acquired during Eoarchean metamorphism at 3.69 Ga (1, 33). The passed pseudo-baked contact tests in metamorphic zones A and B suggest the magnetization in the BIF was not overprinted by Neoarchean or Paleoproterozoic metamorphism. The convergence of directions in two antipodal directions after tilt correction confirms the magnetization was acquired prior to tilting at 3.65–3.60 Ga (29). The consistent southward direction recovered in the baked BIF in geographic coordinates (Figure 2) supports our hypothesis that this magnetization was acquired during Ameralik dyke emplacement 3.26–3.5 Ga, and following tilting. The angular dispersion recovered from the unbaked BIF directions at Site C, our best constrained site, is 21° which is comparable to present-day secular variation (78).

We have shown that paleomagnetic directions in the BIF can be constrained with sufficient confidence to pass our pseudo-baked contact tests with 95% confidence (Figure 2). We note that anisotropy in BIFs, which is predominantly in the plane of the bands (27), will act to rotate both the unbaked and baked directions into the plane of banding. At each field site studied here, samples were preferentially taken from undeformed bands, and the planar orientation of the bands is approximately constant across each site (as described by our basal bedding measurements). Therefore, any anisotropy correction could be assumed to act to correct all recovered directions in the same way. This will have two effects: first, to focus the recovered directions towards the pole to the plane of banding, reducing the scatter in the observed measurements and second, to increase the angle between recovered baked and unbaked directions in our pseudo-baked contact tests since it will remove the bias that pulls both directions into the plane of the bands, thereby improving the confidence to which they pass.

The high degree of scatter in the recovered directions can be explained by the fact that magnetite grain growth took place over a long time period during metamorphism and therefore remanence was acquired at different times by different populations of grains throughout metamorphism. This may indicate that the scatter in the BIF reflects secular variation of the ancient magnetic field. Our paleodirectional results also suggest the Eoarchean geodynamo may have been reversing. The observed convergence of tilt-corrected results in two antipodal directions (Figure 3) is consistent with a reversing field. Given the uncertainty in the relative timing of remanence acquisition between sites A/8A, C and 6A during metamorphism we cannot constrain a possible reversal rate.

We interpret our paleointensity results as evidence for the presence of a geomagnetic field during the Eoarchean. Our paleointensity estimates are similar to those reported by previous studies from the Archean and Hadean (Figure 4), although we note that the vast majority of paleointensity estimates are acquired from single crystals (17, 74, 79) and there is debate over the age of remanence in some of these studies (25, 26, 80). The oldest previous whole-rock paleointensity study was carried out on dacites from the Duffer formation, Australia (19). The authors recovered a paleointensity of 6.4 ± 0.68 μT. They attribute this weak paleointensity to inefficiency in remanence acquisition via a thermo-chemical remanent magnetization (TCRM). The recovered paleointensity record is also difficult to interpret given that weaker intensities could also be attributed to acquisition at low-latitudes (the paleolatitude of the continents during the Archean is unknown) or decreased stability of the geomagnetic field in terms of reversal frequency and secular variation resulting in a weaker average geomagnetic field value.

Our results are consistent with previous studies that suggest the Earth's geomagnetic field has been active since the Eoarchean (21, 79). Given the slow cooling rates post-metamorphism, it is likely that our paleointensity estimate represents a time-averaged field and may have been further reduced from the 'true' value of the geomagnetic field by reversals, on top of the inefficiency associated with remanence acquisition. Therefore we cannot rule out that the Archean magnetic field was at least as strong as Earth's magnetic field today. This highlights current challenges in accurately recovering the strength and stability of the geomagnetic field over Earth's history, although our results suggest behaviour of the Eoarchean geomagnetic field was similar to that observed today. Recent dynamo models have predicted the magnetic field declined in intensity from the Archean until the Ediacaran (81) immediately prior to inner core nucleation. Further constraints on the stability of the Archean field and how this behaviour is manifest in the recovered paleointensity estimates will be required to properly characterize paleointensity trends on billion year timescales.

The paleomagnetic record suggests that Earth has been surrounded by a protective magnetosphere since life originated on its surface. However, our recovered paleointensity of > 15 μT is equivalent to a virtual dipole moment of 1.6×10^{22} Am^2, suggesting a solar wind standoff distance $\sim$ 5 Earth radii, consistent with previous results (82). This is approximately half of the standoff distance provided by Earth's magnetosphere today, although we acknowledge our results represent a lower estimate. Recent models have also shown that a weak intrinsic magnetic field can act to increase atmospheric escape via outflow along open magnetic field lines in the polar regions (polar wind) (4, 5). The degree of atmospheric escape is therefore a trade-off between a larger magnetosphere creating a greater standoff distance that protects the atmosphere from erosion, versus greater connection of open magnetic field lines with the interplanetary magnetic field and increased interaction between the solar wind and atmosphere in the cusp region both of which enhance escape (83, 84).

Given the uncertainty in the exact strength of Earth's magnetic field through time and the unknown reversal rate, the delicate balance between magnetic field strength and atmospheric escape could easily be tipped in favour of net atmospheric loss in the presence of a stronger solar wind during the Archean. Further studies should focus on constraining reliable paleointensities in the Archean. Whole-rock, orientable specimens with magnetization ages constrained by U-Pb dating of magnetite should allow time-resolved paleointensity records to be recovered with sufficient time resolution to interrogate the stability and strength of the geomagnetic field during the Archean now the existence of such a field has been confirmed.

Conclusions

The ISB contains exceptionally well-preserved crustal rocks from the Eoarchean. In particular, the northern-most part of the northeastern end of the belt has only experienced one high temperature (450–550°C) metamorphic and metasomatic episode during the Eoarchean. During this early metamorphic event, magnetite was formed in the BIFs throughout the area with a Pb-Pb age of 3.69 Ga. Between 3.26–3.5 Ga the Ameralik dykes were intruded, and were influenced by a subsequent greenschist-to-amphibolite grade metamorphic event in the late-Archean ca. 2.6 Ga. A third, low temperature metamorphic event occurred 1.5–1.6 Ga. Passed pseudo-baked contacts from 3 sites suggest high-temperature magnetization in the BIF was not reset by either of the subsequent metamorphic events and the BIFs therefore preserve a primary magnetization from the Eoarchean.

Pseudo-Thellier paleointensity results for the BIF recover an Eoarchean geomagnetic field strength of at least $15.1 \pm 1.2\ \mu$T. There is significant uncertainty regarding the type of remanence acquired; when magnetite formed during metamorphism it may have acquired a growth CRM, an alteration CRM or a TCRM and therefore paleointensity estimates likely offer only a lower limit on the true intensity. Paleodirectional results suggest the Eoarchean geomagnetic field experienced reversals and had secular variation similar to the present-day field. Regardless of its exact strength and stability, our results suggest Earth has sustained an intrinsic magnetic field since at least 3.7 Ga. The role of the geomagnetic field in Earth's habitability is presently ambiguous; a magnetosphere can both shield and enhance atmospheric erosion. The solar wind was substantially stronger during the Archean, and therefore the strength of the geomagnetic field and the frequency of reversals will have had a major influence on the stand-off distance created by the magnetosphere and its effectiveness in shielding Earth from atmospheric loss.

Pb-Pb ages from magnetite, which depending on the cooling rate and grain size, can be directly correlated with the magnetization age enable a much larger range of rocks with complex metamorphic histories to be interrogated in future paleomagnetic studies. U-Pb dating combined with paleointensity and paleodirectional studies on Archean whole-rocks from well-constrained stratigraphic sequences will allow the strength and variability of the Archean geomagnetic field to be fully characterised. These observations can then be used to determine the early geomagnetic field's role in shielding Earth's atmosphere from the intense, early solar wind.

Materials and Methods

Paleomagnetic sampling and field tests. Sampling was carried out using a water-cooled Pomeroy EZ Core Drill to extract 2.5-cm-diameter cores. Cores were oriented using a Pomeroy Orienting Fixture and both magnetic and sun compass readings were taken. We primarily relied upon sun compass readings, since the BIF generated strong localized magnetic fields which disturbed magnetic compass readings. Cores were extracted using brass chisels to avoid remagnetizing the specimens.

Conglomerate tests, pseudo-baked contact tests, fold tests and reversal tests were all conducted at various sites within the field area (85, 86). For the conglomerate tests, individual clasts were drilled, as well as the surrounding matrix. For the pseudo-baked contact tests, both the middle and edge of the dykes were drilled, although chilled margins were not obviously visible. The surrounding country rock was drilled at regular intervals of 0.3–1 m, preferentially targeting regions of rock that were absent of fractures, deformation or veining. Specimens were acquired up to > 3 radii from the dyke to ensure sufficient sampling in the unbaked regions. Each area was explored in detail to ensure no other dykes existed close to the unbaked region which may have influenced the recovered paleomagnetic signals. Watson's V_W statistic was used to determine if a distinct direction was acquired close to and far away from each dyke. Both fold and reversal tests were carried out on unbaked BIF directions that passed Watson's V_W test (62).

Paleomagnetic analyses. Drill cores were cut into 1-cm thick discs using the ASC Scientific dual-blade rock saw at MIT. BIF samples were further cut down to 1-mm thick slices using the Buehler IsoMet® low speed saw in the MIT Paleomagnetism Laboratory due to their exceptionally strong magnetic moments. Other lithologies (conglomerate clasts, matrix and Ameralik dykes) were measured as 1-cm thick discs. Specimens were demagnetized using the 2G Enterprises superconducting quantum interference device (SQUID) rock magnetometer, housed in a magnetically-shielded room made of mu-metal with a background DC field of < 200 nT in the MIT Paleomagnetism Laboratory.

Specimens were demagnetized sequentially using several techniques; a subset of specimens were initially placed in liquid nitrogen to remove the majority of the multidomain component (77). In all cases where a liquid nitrogen step was carried out, a sister specimen was also demagnetized without this step in order to ensure this didn't introduce any bias into the recovered data. All specimens were then AF demagnetized in steps of 2 mT from 2–10 mT along three orthogonal axes to 'clean' the specimens of low-coercivity, unstable components. Specimens were then thermally demagnetized between 100–580°C in gradually decreasing temperature steps ranging from 50–5°C. Samples were heated for 1 hour to ensure any magnetization acquired during metamorphic events lasting between 1000 years and 1 Ma was unblocked (87).

Stable components of magnetization were identified using principal component analysis (88). Stable, origin-trending components were defined as those where the maximum angular deviation (MAD) is greater than the deviation angle (dAng). Component directions were plotted in geographic coordinates in Stereonet (89, 90) and Fisher statistics calculated to constrain the mean and α_{95} for each related group of specimens. Where the degree of scatter was large a Watson test for randomness was also conducted (58).

A suite of sister specimens were AF demagnetized along three orthogonal axes from 0–145 mT in steps of 5 mT, with a small subset demagnetized up to 400 mT in steps of 100 mT between 200–400 mT to identify high-coercivity components. Four specimens (A05c, A07c, C02b and D01c) were used for pseudo-Thellier experiments. A 50 μT (50 μT bias DC field applied under a 260 mT alternating field) ARM and 40 mT IRM were imparted to each specimen and then AF demagnetized up to 145 mT. Demagnetization of the ARM was compared to demagnetization of the NRM to calculate paleointensities, B_{anc}, using the following calibration:

$$B_{anc} = \frac{\Delta NRM}{\Delta ARM}\frac{B_{lab}}{a}$$

where $a = 3.28$ is the calibration factor for magnetite (63). For some specimens, the NRM demagnetization had directional components in opposing directions, resulting in substantial curvature in the demagnetization plots. To remove this curvature, vector subtraction was used to isolate the moment magnitude in order to calculate $\frac{\Delta NRM}{\Delta ARM}$. The ARM demagnetization was also compared to the IRM demagnetization to verify the paleointensity recording fidelity of the BIF specimens. The recovered paleointensity, B_{rec}, was estimated using the following:

$$B_{rec} = \frac{\Delta ARM}{\Delta IRM} f$$

where $f = 3000$ (91).

Pb diffusion measurements in magnetite. Lead diffusion in natural magnetite (Fe_3O_4) was characterized over the temperature range 500–675ºC using the powder-source method (92). Magnetite crystals (Moriah, New York, U.S.A.) were sawn into slabs 5–8 mm^2 in area and $\sim$ 1 mm thick using a low-speed diamond saw, with slab orientations parallel to cubic 001 or octahedral 111 forms. One surface of each slab was polished using routine procedures of the Rensselaer Polytechnic Institute laboratory that have been demonstrated to yield surfaces free of dislocations and other lattice damage (93).

A mixture of $PbSO_4$ and Fe_2O_3 (1:1 mass proportions) was prepared for use as a powder source to provide Pb^{2+} ions at the surfaces of the magnetite crystals for diffusive exchange with Fe^{2+} in the magnetite. The combination of Fe_2O_3 in the source and the magnetite samples themselves constituted a solid-state oxygen fugacity buffer (magnetite-hematite; MH), ensuring that the stable oxidation of Pb during the diffusion experiments was 2+, as expected in natural settings where both magnetite and hematite are present.

Preparation for a diffusion experiment involved packing a polished magnetite slab in $PbSO_4$-Fe_2O_3 powder source at the presealed end of a silica-glass tube, which was then evacuated with a mechanical pump and sealed off with an H2-O2 torch. This enclosed, fO_2-buffered system (SiO_2 ampoule and contents) was suspended in a vertical-tube furnace and held at temperature for a preset duration to allow Pb^{2+} from the source to exchange diffusively with Fe^{2+} from the magnetite. The diffusion experiment was terminated by removing the SiO_2 ampoule from the furnace and allowing it to cool in air. The magnetite slab was cleaned of source powder by sonication in ethanol, and Pb uptake was characterized by depth-profiling perpendicular to the surface using Rutherford backscattering spectroscopy (RBS; see 92, 94). Diffusivities were recovered from Pb profiles by fitting the concentration vs. depth data to the solution to the non-steady state diffusion equation for 1-D diffusion into a semi-infinite medium with constant surface concentration. A time series was conducted at 650ºC to ensure that our approach yielded diffusivities independent of experiment duration. U-Pb dating on both apatite and magnetite from the Isua BIF (1, 34, 55) allows useful constraints to be placed on the subsequent thermal histories by considering the Dodson closure temperatures (75) of each of these systems.

ACKNOWLEDGMENTS. CION was funded by the Simons Foundation (grant no. 556352), National Geographic (grant no. EC-50828R-18) and a Lewis and Clark Astrobiology Grant. AE acknowledges support from the MIT EAPS W. O. Crosby and the Johns Hopkins EPS Morton K. Blaustein Postdoctoral Fellowships. SJM, NMK and MJZ were funded by the Collaborative for Research in Origins (CRiO), which was supported by The John Templeton Foundation (principal investigator: Steven Benner/FfAME); the opinions expressed in this publication are those of the authors and do not necessary reflect the views of the John Templeton Foundation. We thank Tim Greenfield for assistance with fieldwork, Jeremy Rushton and Simon Tapster for SEM analysis, Jack Ryan and Richard Harrison for FORC analysis, Matt Beverley-Smith for preparation of polished blocks, Steph Halwa and Rich Palin for assistance with thin section images, and Roger Fishman for drone imagery.

Data Availability Raw data are available for reviewers at Zenodo: https://doi.org/10.5281/zenodo.8052859. All other details of analysis and data interpretation are included in the supplementary materials.

1. R Frei, D Bridgwater, M Rosing, O Stecher, Controversial Pb-Pb and Sm-Nd isotope results in the early Archean Isua (West Greenland) oxide iron formation: Preservation of primary signatures versus secondary disturbances. *Geochimica et Cosmochimica Acta* **63**, 473–488 (1999).
2. JA Tarduno, EG Blackman, EE Mamajek, Detecting the oldest geodynamo and attendant shielding from the solar wind: Implications for habitability. *Phys. Earth Planet. Interiors* **233**, 68–87 (2014).
3. R Lundin, H Lammer, I Ribas, Planetary magnetic fields and solar forcing: Implications for atmospheric evolution. *Space Sci. Rev.* **129**, 245–278 (2007).
4. H Gunell, et al., Why an intrinsic magnetic field does not protect a planet against atmospheric escape. *Astron. Astrophys.* **614**, 1–8 (2018).
5. G Gronoff, et al., Atmospheric Escape Processes and Planetary Atmospheric Evolution. *J. Geophys. Res. Space Phys.* **125**, 1–77 (2020).
6. AJ Biggin, et al., Palaeomagnetic field intensity variations suggest Mesoproterozoic inner-core nucleation. *Nature* **526**, 245–248 (2015).
7. RK Bono, JA Tarduno, F Nimmo, RD Cottrell, Young inner core inferred from Ediacaran ultra-low geomagnetic field intensity. *Nat. Geosci.* **12** (2019).
8. Z Konôpková, RS McWilliams, N Gómez-Pérez, AF Goncharov, Direct measurement of thermal conductivity in solid iron at planetary core conditions. *Nature* **534**, 99–101 (2016).
9. K Ohta, Y Kuwayama, K Hirose, K Shimizu, Y Ohishi, Experimental determination of the electrical resistivity of iron at Earth's core conditions. *Nature* **534**, 95–98 (2016).
10. M Pozzo, C Davies, D Gubbins, D Alfè, Thermal and electrical conductivity of iron at Earth's core conditions. *Nature* **485**, 355–358 (2012).
11. Y Zhang, et al., Reconciliation of Experiments and Theory on Transport Properties of Iron and the Geodynamo. *Phys. Rev. Lett.* **125** (2020).
12. JG O'Rourke, DJ Stevenson, Powering Earth's dynamo with magnesium precipitation from the core. *Nature* **529**, 387–389 (2016).
13. J Badro, J Siebert, F Nimmo, An early geodynamo driven by exsolution of mantle components from Earth's core. *Nature* **536**, 326–328 (2016).
14. K Hirose, et al., SiO2 crystallization and compositional evolution of the Earth's core. *Nature* pp. 2–12 (2016).
15. NA Blanc, DR Stegman, LB Ziegler, Thermal and magnetic evolution of a crystallizing basal magma ocean in Earth's mantle. *Earth Planet. Sci. Lett.* **534**, 116085 (2020).
16. M Landeau, A Fournier, HC Nataf, D Cébron, N Schaeffer, Sustaining Earth's magnetic dynamo. *Nat. Rev. Earth Environ.* **0123456789** (2022).
17. JA Tarduno, et al., Geodynamo, solar wind, and magnetopause 3.4 to 3.45 billion years ago. *Science* **327**, 1238–1240 (2010).
18. AJ Biggin, et al., Palaeomagnetism of Archaean rocks of the Onverwacht Group, Barberton Greenstone Belt (southern Africa): Evidence for a stable and potentially reversing geomagnetic field at ca. 3.5Ga. *Earth Planet. Sci. Lett.* **302**, 314–328 (2011).
19. E Herrero-Bervera, D Krasa, MJ Van Kranendonk, A whole rock absolute paleointensity determination of dacites from the Duffer Formation (ca. 3.467 Ga) of the Pilbara Craton, Australia: An impossible task? *Phys. Earth Planet. Interiors* **258**, 51–62 (2016).
20. Ja Tarduno, RD Cottrell, WJ Davis, F Nimmo, RK Bono, Supplementary Material for A Hadean to Paleoarchean geodynamo recorded by single zircon crystals. **521** (2015).
21. JA Tarduno, et al., Paleomagnetism indicates that primary magnetite in zircon records a strong Hadean geodynamo. *Proc. Natl. Acad. Sci.* pp. 1–10 (2020).
22. F Tang, et al., Secondary magnetite in ancient zircon precludes analysis of a Hadean geodynamo. *Proc. Natl. Acad. Sci.* **116**, 407–412 (2019).
23. BP Weiss, et al., Pervasive remagnetization of detrital zircon host rocks in the Jack Hills, Western Australia and implications for records of the early geodynamo. *Earth Planet. Sci. Lett.* **430**, 115–128 (2015).
24. BP Weiss, et al., Secondary magnetic inclusions in detrital zircons from the Jack Hills , Western Australia and implications for the origin of the geodynamo microscopy. *Geology* **46** (2018).
25. C Borlina, et al., Re-evaluating the evidence for a Hadean-Eoarchean dynamo. *Sci. Adv.* **6**, 1–9 (2020).
26. RJ Taylor, et al., Direct age constraints on the magnetism of Jack Hills zircon. *Sci. advances* **9**, eadd1511 (2023).
27. PW Schmidt, DA Clark, Palaeomagnetism and magnetic anisotropy of proterozoic banded-iron formations and iron ores of the Hamersley Basin Western Australia. *Explor. Geophys.* **24**, 223–226 (1994).
28. H Wabo, et al., Mineral transformations during thermal demagnetization of sideritic jasper mesobands in jaspilites of the $\sim$3.25 ga fig tree group in the barberton greenstone belt, kaapvaal craton (South Africa). *South Afr. J. Geol.* **121**, 131–140 (2018).
29. AP Nutman, CR Friend, New 1:20,000 scale geological maps, synthesis and history of investi-

gation of the Isua supracrustal belt and adjacent orthogneisses, southern West Greenland: A glimpse of Eoarchaean crust formation and orogeny. *Precambrian Res.* **172**, 189–211 (2009).
30. B Rasmussen, JR Muhling, Making magnetite late again: Evidence for widespread magnetite growth by thermal decomposition of siderite in Hamersley banded iron formations. *Precambrian Res.* **306**, 64–93 (2018).
31. KO Konhauser, et al., Iron formations: A global record of Neoarchaean to Palaeoproterozoic environmental history. *Earth-Science Rev.* **172**, 140–177 (2017).
32. AP Nutman, VC Bennett, CR Friend, Seeing through the magnetite: Reassessing Eoarchean atmosphere composition from Isua (Greenland) 3.7 Ga banded iron formations. *Geosci. Front.* **8**, 1233–1240 (2017).
33. RF Dymek, C Klein, Chemistry , Petrology and Origin of Banded Iron- Formation Lithologies From the 3800 Ma Isua Supracrustal Belt , West Greenland. *Precambrian Res.* **39**, 247–302 (1988).
34. R Frei, A Polat, Source heterogeneity for the major components of 3.7 Ga Banded Iron Formations (Isua Greenstone Belt, Western Greenland): Tracing the nature of interacting water masses in BIF formation. *Earth Planet. Sci. Lett.* **253**, 266–281 (2007).
35. K Kobayashi, Chemical Remanent Magnetization of Ferromagnetic Minerals and its Application to Rock Magnetism. *J. geomagnetism geoelectricity* **10**, 99–117 (1959).
36. LB Stokking, L Tauxe, Acquisition of chemical remanent magnetization by synthetic iron oxide. *Nature* pp. 18–20 (1987).
37. LB Stokking, L Tauxe, Properties of chemical remanence in synthetic hematite: Testing theoretical predictions. *J. Geophys. Res.* **95**, 639–652 (1990).
38. I Halevy, Y Feldman, R Popovitz-Biro, EM Schuster, M Alesker, A key role for green rust in the Precambrian oceans and the genesis of iron formations. *Nat. Geosci.* **10**, 135–139 (2017).
39. JE Johnson, JR Muhling, J Cosmidis, B Rasmussen, AS Templeton, Low-Fe(III) Greenalite Was a Primary Mineral From Neoarchean Oceans. *Geophys. Res. Lett.* **45**, 3182–3192 (2018).
40. NJ Tosca, S Guggenheim, PK Pufahl, An authigenic origin for Precambrian greenalite: Implications for iron formation and the chemistry of ancient seawater. *Bull. Geol. Soc. Am.* **128**, 511–530 (2016).
41. Y Erel, Y Harlavan, M Stein, JD Blum, U-Pb dating of Fe-rich phases using a sequential leaching method. *Geochimica et Cosmochimica Acta* **61**, 1697–1703 (1997).
42. S Gelcich, DW Davis, ET Spooner, Testing the apatite-magnetite geochronometer: U-Pb and 40Ar/ 39Ar geochronology of plutonic rocks, massive magnetite-apatite tabular bodies, and IOCG mineralization in Northern Chile. *Geochimica et Cosmochimica Acta* **69**, 3367–3384 (2005).
43. EB Watson, DJ Cherniak, CIO Nichols, BP Weiss, Pb diffusion in magnetite: dating magnetite crystallization and the timing of remanent magnetization in banded iron formation. *Chem. Geol.* (2023).
44. AP Nutman, CR Friend, VC Bennett, K Yi, M Van Kranendonk, Review of the Isua supracrustal belt area (Greenland) Eoarchean geology from integrated 1:20,000 scale maps, field observations and laboratory data: Constraints on early geodynamics. *Precambrian Res.* **379**, 106785 (2022).
45. T Arai, S Omori, T Komiya, S Maruyama, Intermediate P / T-type regional metamorphism of the Isua Supracrustal Belt , southern west Greenland : The oldest Paci fi c-type orogenic belt ? *Tectonophysics* **662**, 22–39 (2015).
46. T Komiya, M Hayashi, S Maruyama, H Yurimoto, Intermediate-P/T type Archean metamorphism of the Isua supracrustal belt: Implications for secular change of geothermal gradients at subduction zones and for Archean plate tectonics. *Am. J. Sci.* **302**, 806–826 (2002).
47. H Rollinson, The metamorphic history of the Isua Greenstone Belt, West Greenland. *Geol. Soc. London, Special Publ.* **199**, 329–350 (2002).
48. H Rollinson, Metamorphic history suggested by garnet-growth chronologies in the Isua Greenstone Belt, West Greenland. *Precambrian Res.* **126**, 181–196 (2003).
49. S Aoki, C Kabashima, Y Kato, T Hirata, T Komiya, Influence of contamination on banded iron formations in the Isua supracrustal belt, West Greenland: Reevaluation of the Eoarchean seawater compositions. *Geosci. Front.* **9**, 1049–1072 (2016).
50. AP Nutman, CRL Friend, VC Bennett, VR MCGregor, Dating of the Ameralik dyke swarms of the Nuuk district, southern West Greenland: mafic intrusion events starting from c. 3510 Ma. *J. Geol. Soc.* **161**, 421–430 (2004).
51. AP Nutman, H Hagiya, S Maruyama, AP Nutman, SHRIMP U-Pb single zircon geochronology of a Proterozoic mafic dyke, Isukasia, southern West Greenland. *Bull. Geol. Soc. Denmark* **42**, 17–2210 (1995).
52. R Frei, D Bridgwater, M Rosing, O Stecher, Controversial Pb-Pb and Sm-Nd isotope results in the early Archean Isua (West Greenland) oxide iron formation: Preservation of primary signatures versus secondary disturbances. *Geochimica et Cosmochimica Acta* **63**, 473–488 (1999).
53. A Polat, AW Hofmann, C Münker, M Regelous, PW Appel, Contrasting geochemical patterns in the 3.7-3.8 Ga pillow basalt cores and rims, Isua greenstone belt, Southwest Greenland: Implications for postmagmatic alteration processes. *Geochimica et Cosmochimica Acta* **67**, 441–457 (2003).
54. T Komiya, S Maruyama, T Hirata, H Yurimoto, S Nohda, Geochemistry of the oldest MORB and OIB in the Isua Supracrustal Belt, southern West Greenland: Implications for the composition and temperature of early Archean upper mantle. *Island Arc* **13**, 47–72 (2004).
55. M Nishizawa, et al., Rare-earth element, lead, carbon, and nitrogen geochemistry of apatite-bearing metasediments from the similar to 3.8 Ga Isua supracrustal belt, West Greenland. *Int. Geol. Rev.* **47**, 952–970 (2005).
56. W Lowrie, M Fuller, On the alternating field demagnetization characteristics of multidomain thermoremanent magnetization in magnetite. *J. Geophys. Res.* **76**, 6339–6349 (1971).
57. JP Hodych, Magnetostrictive control of coercive force in multidomain magnetite. *Nature* **298**, 542–544 (1982).
58. GS Watson, A test for randomness of directions. *Geophys. Suppl. to Mon. Notices Royal Astron. Soc.* **7**, 160–161 (1965).
59. RV White, JL Crowley, JS Myers, Earth ' s oldest well-preserved mafic dyke swarms in the vicinity of the Isua greenstone belt , southern West Greenland. *Episodes* **72**, 65–72 (2000).
60. GS Watson, Large sample theory of the Langevin distribution. *J. Stat. Plan. Inference* **8**, 245–256 (1983).
61. L Tauxe, GS Watson, The fold test: an eigen analysis approach. *Earth Planet. Sci. Lett.* **122**, 331–341 (1994).
62. L Tauxe, N Kylstra, C Constable, Bootstrap statistics for paleomagnetic data. *J. Geophys. Res.* **96**, 11723–11740 (1991).
63. GA Paterson, D Heslop, Y Pan, The pseudo-Thellier palaeointensity method: New calibration and uncertainty estimates. *Geophys.* **207**, 1596–1608 (2016).
64. PA Selkin, JS Gee, L Tauxe, WP Meurer, AJ Newell, The effect of remanence anisotropy on paleointensity estimates: A case study from the Archean Stillwater Complex. *Earth Planet. Sci. Lett.* **183**, 403–416 (2000).
65. RK Bono, et al., The PINT database: A definitive compilation of absolute palaeomagnetic intensity determinations since 4 billion years ago. *Geophys. J. Int.* pp. 522–545 (2021).
66. aR Muxworthy, ME Evans, SJ Scourfield, JG King, Paleointensity results from the late-Archaean Modipe Gabbro of Botswana. *Geochem. Geophys. Geosystems* **14**, 2198–2205 (2013).
67. AJ Biggin, GH Strik, CG Langereis, The intensity of the geomagnetic field in the late-Archaean: New measurements and an analysis of the updated IAGA palaeointensity database. *Earth, Planets Space* **61**, 9–22 (2009).
68. C Morimoto, YI Otofuji, M Miki, H Tanaka, T Itaya, Preliminary palaeomagnetic results of an Archaean dolerite dyke of west Greenland: Geomagnetic field intensity at 2.8 Ga. *Geophys. J. Int.* **128**, 585–593 (1997).
69. PA Selkin, JS Gee, WP Meurer, SR Hemming, Paleointensity record from the 2.7 Ga Stillwater Complex, Montana. *Geochem. Geophys. Geosystems* **9** (2008).
70. PA Selkin, L Tauxe, Long-term variations in palaeointensity. *Philos. Transactions Royal Soc. A: Math. Phys. Eng. Sci.* **358**, 1065–1088 (2000).
71. A Yoshihara, Y Hamano, Intensity of the Earth's magnetic field in late Archean obtained from diabase dikes of the Slave Province, Canada. *Phys. Earth Planet. Interiors* **117**, 295–307 (2000).
72. M Miki, et al., Palaeomagnetism and geochronology of the proterozoic dolerite dyke from southwest greenland: Indication of low palaeointensity. *Geophys. J. Int.* **179**, 18–34 (2009).
73. VV Shcherbakova, NV Lubnina, VP Shcherbakov, GV Zhidkov, VA Tsel'movich, Paleointensity determination on Neoarchaean dikes within the Vodlozerskii terrane of the Karelian craton. *Izvestiya, Phys. Solid Earth* **53**, 714–732 (2017).
74. Ja Tarduno, RD Cottrell, MK Watkeys, D Bauch, Geomagnetic field strength 3.2 billion years ago recorded by single silicate crystals. *Nature* **446**, 657–660 (2007).
75. MH Dodson, Closure temperature in cooling geochronological and petrological systems. *Contributions to Mineral. Petrol.* **40**, 259–274 (1973).
76. CJ Warren, SP Kelley, SC Sherlock, CS McDonald, Metamorphic rocks seek meaningful cooling rate: Interpreting 40Ar/39Ar ages in an exhumed ultra-high pressure terrane. *Lithos* **155**, 30–48 (2012).
77. SL Halgedahl, RD Jarrard, Low-temperature behavior of single-domain through multidomain magnetite. *Earth Planet. Sci. Lett.* **130**, 127–139 (1995).
78. SP Lund, A new view of long-term geomagnetic field secular variation. *Front. Earth Sci.* **6**, 1–13 (2018).
79. JA Tarduno, RD Cottrell, WJ Davis, F Nimmo, RK Bono, A Hadean to Paleoarchean geodynamo recorded by single zircon crystals. *Science* (2015).
80. M Tang, CTA Lee, G Costin, HE Höfer, Recycling reduced iron at the base of magmatic orogens. *Earth Planet. Sci. Lett.* **528**, 115827 (2019).
81. CJ Davies, et al., Dynamo constraints on the long-term evolution of Earth's magnetic field strength. *Geophys. J. Int.* **228**, 316–336 (2022).
82. JA Tarduno, EG Blackman, EE Mamajek, Detecting the oldest geodynamo and attendant shielding from the solar wind: Implications for habitability. *Phys. Earth Planet. Interiors* **233**, 68–87 (2014).
83. AA Vidotto, *The evolution of the solar wind.* (Springer International Publishing) Vol. 18, pp. 1–86 (2021).
84. EG Blackman, JA Tarduno, Mass and energy capture from stellar winds for magnetized and unmagnetized planets: implications for atmospheric erosion and habitability. (2018).
85. K Buchan, Baked Contact Test in *Encyclopedia of Geomagnetism and Paleomagnetism*, eds. D Gubbins, E Herrero-Bervera. (Springer, Dordrecht), pp. 35–55 (2007).
86. JW Graham, The stability and significance of magnetism in sedimentary rocks. *J. Geophys. Res.* **54**, 131–167 (1949).
87. G Pullaiah, E Irving, K Buchan, D Dunlop, Magnetization changes caused by burial and uplift. *Earth Planet. Sci. Lett.* **28**, 133–143 (1975).
88. JL Kirschvink, The least-squares line and plane and the analysis of palaeomagnetic data. *Geophys. J. R. Astr. Soc.* **62**, 699–718 (1980).
89. RW Allmendinger, NC Cardozo, D Fisher, Vectors Tensors in *Structural Geology Algorithms.* (Cambridge University Press), pp. 44–98 (2013).
90. NC Cardozo, RW Allmendinger, Spherical projections with OSXStereonet. *Comput. Geosci.* **51**, 193–205 (2013).
91. J Gattacceca, P Rochette, Toward a robust normalized magnetic paleointensity method applied to meteorites. *Earth Planet. Sci. Lett.* **227**, 377–393 (2004).
92. EB Watson, R Dohmen, Non-traditional and emerging methods for characterizing diffusion in minerals and mineral aggregates. *Rev. Mineral. Geochem.* **72**, 61–105 (2010).
93. EB Watson, DJ Cherniak, JB Thomas, JM Hanchar, R Wirth, Crystal surface integrity and diffusion measurements on Earth and planetary materials. *Earth Planet. Sci. Lett.* **450**, 346–354 (2016).
94. DJ Cherniak, R Hervig, J Koepke, Y Zhang, D Zhao, Analytical methods in diffusion studies. *Rev. Mineral. Geochem.* **72**, 107–170 (2010).